Neuropharmacology 282 (2026) 110724

Contents lists available at ScienceDirect

Neuropharmacology

journal homepage: www.elsevier.com/locate/neuropharm

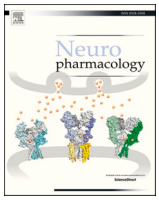

Adenosine A_{2A} receptor blockade promotes oligodendrocyte differentiation and myelination: Highlighting the potency of an edaravone-conjugated A_{2A} receptor antagonist

F. Cherchi [a,1,*], L. Frulloni [a], M. Venturini [a], G. Magni [b], S. Calenda [c], R. Innocenti [d], F. Varano [c], D. Catarzi [c], C. Ceni [c], G. Vagnoni [c], V. Colotta [c], F. Vincenzi [e], K. Varani [e], M. Prisinzano [d], C. Donati [d], F. Cencetti [d], E. Coppi [a], A.M. Pugliese [a,*]

[a] Section of Pharmacology and Toxicology, Department of Neuroscience, Psychology, Drug Research and Child Health (NEUROFARBA), University of Florence, Florence, Italy
[b] Istituto di Fisica Applicata "Nello Carrara", Consiglio Nazionale Delle Ricerche (CNR-IFAC), Sesto Fiorentino, Italy
[c] Section of Pharmaceutical and Nutraceutical Sciences, Department of NEUROFARBA, University of Florence, Florence, Italy
[d] Department of Experimental and Clinical Biomedical Sciences, University of Florence, Florence, Italy
[e] Department of Translational Medicine, University of Ferrara, Ferrara, Italy

ARTICLE INFO

Keywords:
Adenosine A_{2A} receptors
Oligodendroglial cells
Patch-clamp
Myelin
Remyelination
Antioxidant
Multitarget drugs

ABSTRACT

Many neurodegenerative diseases, including demyelinating pathologies, are characterized by complex pathological processes mediated by multiple damage mechanisms. While current drugs predominantly target oxidative stress pathways, understanding multi-target modulation could clarify mechanisms underlying demyelination. This study aimed to explore the pharmacological effects of different selective adenosine A_{2A} receptor antagonists, alone or conjugated with antioxidant edaravone, on oligodendrogliogenesis and myelination processes in purified rat cultured oligodendrocyte precursor cells (OPCs) or co-cultured with rat dorsal root ganglion neuron, respectively. We hypothesize that simultaneously targeting adenosine A_{2A} receptor signalling and oxidative stress pathways may enhance oligodendrocyte differentiation and promote myelination. To this purpose, we used patch-clamp recordings, antioxidant assay, quantitative real-time PCR and the OPC/dorsal root ganglion neuron co-culture. Selective A_{2A} receptor activation inhibited voltage-dependent K^+ currents in cultured OPCs, an effect strictly correlated with their differentiation and prevented by the thiazolopyrimidine adenosine A_{2A} receptor antagonists. The block of these receptors promoted OPC differentiation, as determined by measuring total myelin basic protein (MBP) expression, and counteracted the increase in reactive oxygen species levels induced by oxidative stress in purified cultured OPCs. Among all compounds tested, only the edaravone hybrid derivative P686 enhanced myelination in OPC/dorsal root ganglion neuron co-cultures, quantified by the Mander's coefficient which reflects the overlap between MBP^+-pixels and the neuronal marker βIII-tubulin$^+$-pixels. These results provide mechanistic insight into how multitarget modulation of A_{2A} receptor signalling and oxidative stress regulates oligodendrocyte differentiation and myelination, highlighting avenues for future studies rather than therapeutic application in support demyelinating diseases.

1. Introduction

Oligodendrocytes, the myelin-forming glial cells within the central nervous system (CNS), are responsible for the formation and maintenance of myelin sheaths, which are essential for the rapid conduction of electrical impulses along axons. Loss of myelin integrity is a hallmark of various demyelinating diseases, including multiple sclerosis (MS) and amyotrophic lateral sclerosis (ALS). Recent research highlights the importance of targeting both oxidative stress and receptor-mediated signalling to improve oligodendrocyte survival and promote

This article is part of a special issue entitled: Tribute to Francesco Di Virgilio published in Neuropharmacology.

* Corresponding authors.
E-mail addresses: federica.cherchi@unifi.it, federica.cherchi@meyer.it (F. Cherchi).
[1] Department of Neuroscience and Medical Genetics, Meyer Children's Hospital IRCCS, Florence, Italy. (present address).

https://doi.org/10.1016/j.neuropharm.2025.110724
Received 8 July 2025; Received in revised form 8 September 2025; Accepted 13 October 2025
Available online 19 October 2025

myelination, a process that is impaired in demyelinating diseases (Cherchi et al., 2021a; Miller and Wachowicz, 2013; Spaas et al., 2021).

Adenosine, a purine nucleoside, acts as a neuromodulator in both the immune system and the CNS, exerting its effects through its metabotropic receptors (A_1R, $A_{2A}R$, $A_{2B}R$, A_3R) (Antonioli et al., 2013). These receptors are expressed at all stages of oligodendrocyte development (Fields, 2004; Stevens et al., 2002) and play a crucial role during their differentiation and maturation (Cherchi et al., 2021b). The $A_{2A}R$ subtype, in particular, regulates oligodendrocyte precursor cell (OPC) differentiation. Activation of $A_{2A}R$ by the selective agonist CGS21680 inhibits I_K currents necessary to OPC maturation (Coppi et al., 2013; Gallo et al., 1996), delaying differentiation without affecting cell viability or proliferation, an effect entirely reversed by the $A_{2A}R$ antagonist SCH58261 (Coppi et al., 2013), confirming the involvement of $A_{2A}R$ signalling in oligodendrogliogenesis. Upregulation of $A_{2A}Rs$ has been observed in the cerebral white matter of MS patients (Rissanen et al., 2013) and in the corresponding mouse model, experimental autoimmune encephalomyelitis (EAE; Mills et al., 2012), correlating with disease severity. Modulation of $A_{2A}Rs$ in EAE mice has yielded divergent results depending on timing of administration during disease progression and target cell type. The activation of $A_{2A}R$ proved anti-inflammatory effects when administered in the early phase of EAE, leading to prevention of disease symptoms by suppressing T-cell infiltration, proliferation and cytokine release (Ingwersen et al., 2016; Yao et al., 2012). Conversely, if administered after symptoms exordium, $A_{2A}R$ agonists promote disease progression and exacerbate neurological impairment (Ingwersen et al., 2016) whereas antagonists protected from demyelination and microglial activation (Chen et al., 2019).

In a cuprizone animal model of demyelination the $A_{2A}R$ knockout mice displayed a significant increased expression of myelin basic protein (MBP) (Adebiyi and Bynoe, 2023), indicating their beneficial role in myelin regulation. These findings suggest that $A_{2A}Rs$ exert dual and context-dependent roles in demyelinating disorders, with receptor blockade offering a promising strategy to enhance oligodendrocyte regeneration in the remyelination phase.

Edaravone, an FDA-approved antioxidant (U.S. Food and Drug Administration, 2022) for ALS, has gained attention for its neuroprotective properties, particularly in conditions characterized by oxidative stress. Moreover, in Japan many patients with acute ischemic stroke have been treated with edaravone since 2001 showing improvement of neurological symptoms and functional impairment associated with acute focal injury (Agresti et al., 2019; Otomo et al., 2003).

This compound scavenges reactive oxygen species (ROS), which are implicated in neurodegeneration and demyelination across various neuropathological conditions. Beyond its antioxidant effects, edaravone activates intracellular signalling pathways such as the nuclear factor E2-related factor 2 (NRF2), which regulates the expression of genes involved in detoxification and ROS homeostasis (Watanabe et al., 2018). It also inhibits the release of pro-inflammatory cytokines by suppressing NFκB activation in various experimental models, such as in the brains of mice with hepatic encephalopathy (Jangra et al., 2016) and in the hippocampus of rats with cisplatin-induced neurotoxicity (Amirshahrokhi and Imani, 2025). Importantly, edaravone has been shown to promote remyelination in various in vitro and in vivo models, including those of MS, by enhancing OPC differentiation and accelerating the rate of myelination (Bakhtiari et al., 2021; Eleuteri et al., 2017). It has also been shown to improve OPC differentiation and remyelination in neuromyelitis optica spectrum disorder (NMOSD) (Luo et al., 2023).

This paper investigates the effects of $A_{2A}R$ antagonists on OPC cultures, including compounds featuring a thiazolo[5,4 d]pyrimidine core structure, i.e. the previously reported derivatives P625 (compound **8** in (Varano et al., 2020b) and P400 (compound **14** in (Varano et al., 2016), as well as the novel compound P686 (Fig. 1).

P686 is a hybrid derivative of P400 and edaravone, recently synthesized (see Methods) to create a dual-target agent capable of blocking $A_{2A}R$ while also retaining the properties of edaravone, primarily its antioxidant activity. As expected, P686 proved to be a potent $A_{2A}R$ antagonist with good selectivity versus the other AR subtypes (Table I).

To better contextualize their activity, we compared the thiazolopyrimidine derivatives to a commercially available $A_{2A}R$ antagonist and to edaravone alone. We hypothesize that simultaneously targeting $A_{2A}R$ signalling and oxidative stress pathways may enhance oligodendrocyte differentiation and promote myelination. To test this, we employed a combination of experimental approaches, including patch-clamp recordings, antioxidant assays, quantitative real-time PCR, and the OPC/

Table I
Affinity and potency of derivative P686 at hARs [a] Data are expressed as means ± SEM. Affinity values obtained from displacement of [^{3}H] DPCPX [b], [^{3}H] ZM241385 [c] or [^{125}I] ABMECA [f] specific binding to human (h) A_1Rs, $hA_{2A}R$ or hA_3R, respectively (n = 3–6). [d]Potency (IC_{50}) on cyclic AMP assays in hA_{2A} CHO cells. [e]Potency (IC_{50}) on cyclic AMP assays in hA_{2B} CHO cells.

	hA_1R[b] K_i (nM)	$hA_{2A}R$[c] K_i (nM)	$hA_{2A}R$[d] IC_{50} (nM)	$hA_{2B}R$[e] IC_{50} (nM)	hA_3R[f] K_i (nM)
P686	805 ± 66	36.3 ± 2.8	41.3 ± 3.2	413 ± 33	4092 ± 315

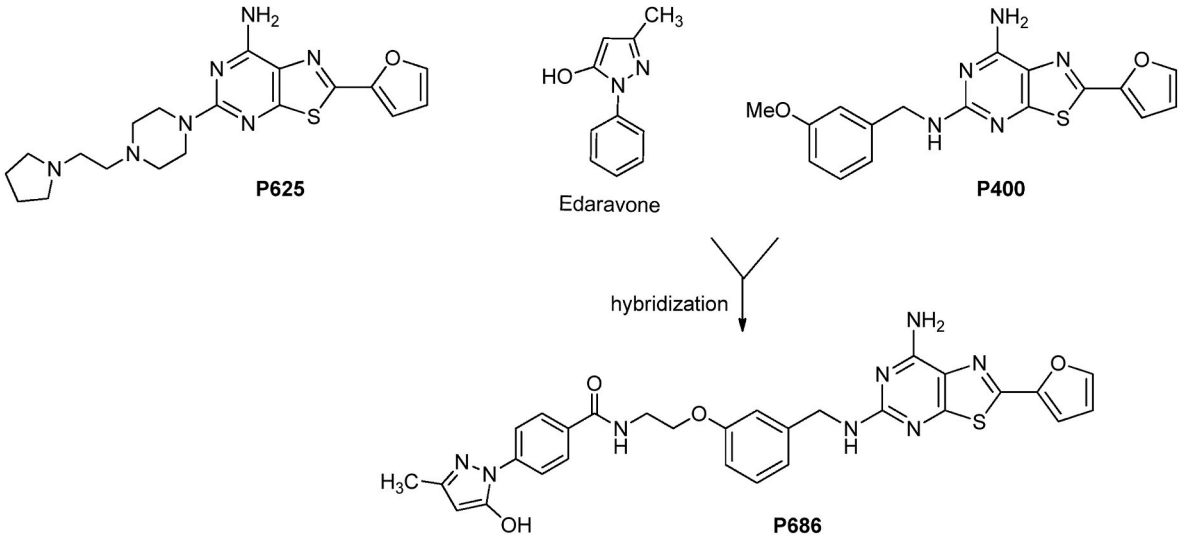

Fig. 1. Structures of edaravone and the herein investigated $A_{2A}R$ antagonists.

dorsal root ganglion neuron (DRGN) co-culture model to evaluate myelination. Our results demonstrate that while all $A_{2A}R$ antagonists promote OPC differentiation, the edaravone hybrid derivative P686 exert superior effects by also enhancing myelination in OPC/DRGN co-cultures. These findings support the potential of multitarget compounds as promising therapeutic candidates for the treatment of demyelinating diseases such as MS and ALS.

2. Materials and methods

2.1. Chemistry

Analytical silica gel plates (0.20 mm, F254, Merck, Germany) and silica gel 60 (Merck, 70–230 mesh) were used for analytical and column chromatography, respectively. All melting points were determined on a Gallenkamp melting point apparatus and were uncorrected. Elemental analyses were performed with a Flash E1112 Thermofinnigan elemental analyzer for C, H, N and the results were within 0.4 % of the theoretical values. All compounds revealed purity not less than 95 %. NMR spectra were recorded on a Bruker Avance 400 spectrometer (400 MHz for ^{1}H- and 100 Mz for ^{13}C- NMR). The chemical shifts are reported in δ (ppm) and are relative to the central peak of the solvent, which was $CDCl_3$ or $DMSOd_6$. The following abbreviations are used: s = singlet, d = doublet, t = triplet, q = quartet, m = multiplet, br = broad, and ar = aromatic protons.

The thiazolopyrimidine **P686** was synthesized starting from compound **1** (Varano F. et al., 2016), which was alkylated with chloroacetonitrile to yield the nitrile derivative **2**. Reaction of **2** with $LiAlH_4$ in anhydrous tetrahydrofuran afforded the corresponding amine derivative **3**. A coupling reaction between compound **3** and edaravone derivative **4** (Gavande et al., 2017), carried out in anhydrous dimethylformamide in the presence of 1-hydroxybenzotriazole and 1-(3-(dimethylamino)propyl)-3-ethylcarbodiimide hydrochloride, gave the desired compound **P686** (see Scheme 1).

2.1.1. Synthesis of 2-(3-(((7-amino-2-(furan-2-yl)thiazolo[5,4-d] pyrimidin-5-yl)amino)methyl)phenoxy)acetonitrile, 2

A suspension of hydroxy derivative **1** (1.92 mmol) (Varano et al., 2016) and K_2CO_3 (3.84 mmol) in anhydrous acetone (30 mL) was stirred at room temperature, under nitrogen atmosphere, for 15 min, then chloroacetonitrile (7.69 mmol) was added and the suspension was reflux for 12 h. The solid was filtered under vacuum, and washed with acetone (50 mL), then the mother liquor was evaporated to dryness under reduced pressure, and the resulting solid was purified by silica gel column chromatography (eluting system: dichloromethane/methanol 9.5:0.5). Yield 70 %. Mp 181–183 °C. ^{1}H NMR (DMSO-d_6) 4.51 (d, 2H, CH_2, J = 6.3 Hz), 5.14 (s, 2H, CH_2), 6.72 (dd, 1H, H furyl, J = 3.5 and 1.8 Hz), 6.93 (dd, 1H, H ar, J = 2.4 and 1.4 Hz), 7.02–7.06 (m, 3H, 2 ar +1 furyl), 7.20 (s, 2H, NH_2, *exchangeable* with D_2O), 7.29–7.33 (m, 1 H, ar), 7.38 (s, 1H, NH, exchangeable with D_2O), 7.90 (d, 1H, furyl, J = 1.2 Hz). Anal. Calcd for ($C_{18}H_{14}N_6O_2S$): C, 57.13; H, 3.73; N, 22.21; Found: C, 57.43; H, 3.90; N, 22.02.

2.1.2. Synthesis of N^5-(3-(2-aminoethoxy)benzyl)-2-(furan-2-yl)thiazolo [5,4-d]pyrimidine-5,7-diamine 3

The nitrile derivative **2** (1.53 mmol) was portion wise added to a stirred suspension of $LiAlH_4$ (6.9 mmol) in anhydrous THF (30 mL), at 0 °C. After the addition was completed, the mixture was stirred at room temperature for 3 h, then treated with ice-cold water (20 mL) followed by ethyl acetate (20 mL). The undissolved white solid was filtered off and the aqueous phase was extracted with ethyl acetate (3 x 20 mL). The combined organic phases were dried (Na_2SO_4) and the solvent removed under reduced pressure to give a solid, which was purified by silica gel column chromatography (eluting system: dicloromethane/methanol/NH_4OH 30 % solution 9:1:0.1). Yield 60 %. Mp 173–175 °C. ^{1}H NMR (DMSO-d_6) 2.70 (brs, 2H, NH_2, exchangeable with D_2O), 2.87–2.89 (m, 2H, CH_2), 3.90–3.93 (m, 2H, CH_2), 4.48 (d, 2H, CH_2, J = 5.8 Hz), 6.72 (s, 1H, furyl), 6.78 (d, 1H, ar, J = 7.6 Hz), 6.88–6.89 (m, 2H, ar), 7.06 (d, 1H, furyl, J = 3.1 Hz), 7.19–7.22 (m, 3H, 1ar + NH_2, exchangeable with D_2O), 7.38 (s, 1H, NH, exchangeable with D_2O), 7.90 (s, 1H, furyl). Anal. Calcd for ($C_{18}H_{18}N_6O_2S$): C, 56.53; H, 4.74; N, 21.97; Found: C, 56.42; H, 4.56; N, 22.02.

2.1.3. Synthesis of N-(2-(3-(((7-amino-2-(furan-2-yl)thiazolo[5,4-d] pyrimidin-5-yl)amino)methyl)phenoxy)ethyl)-4-(5-hydroxy-3-methyl-1H-pyrazol-1-yl)benzamide, P686

Edaravone derivative **4** (0.26 mmol) (Gavande et al., 2017) was reacted with the thiazolopyrimidine derivative **3** (0.29 mmol) in anhydrous DMF (1 mL), in the presence of 1-(3-(dimethylamino)-propyl))-3-ethylcarbodiimide hydrochloride (0.29 mmol) and 1-hydroxybenzotriazole (0.29 mmol), for 24 h at room temperature under nitrogen atmosphere. The mixture was diluted with water (20 mL), and the resulting solid was collected by filtration and purified by silica gel column chromatography (eluting system: cyclohexane/ethyl acetate/methanol 6:4:1). Yield 20 %. Mp: 160–161 °C. ^{1}H NMR (DMSO-d_6) 2.12 (s, 3H, CH_3), 3.62 (d, 2H, CH_2, J = 5.0 Hz), 4.10 (s, 2H,

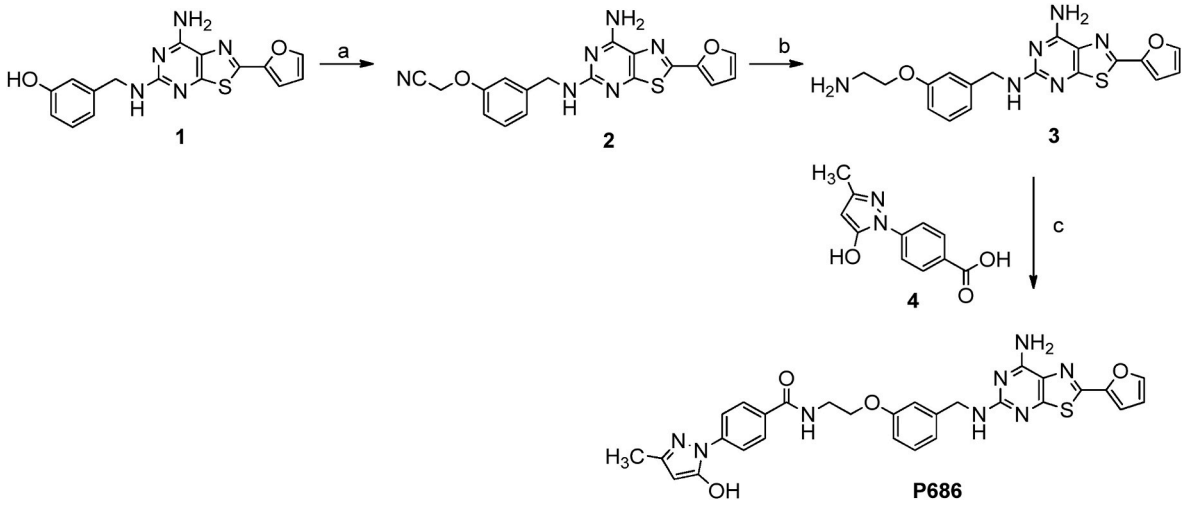

Scheme 1. [a]

[a]Reagents and conditions: a) Chloroacetonitrile, anhydrous K_2CO_3, anhydrous acetone; b) $LiAlH_4$, anhydrous THF; c) 1-hydroxybenzotriazole, 1-(3-(dimethylamino)-propyl))-3-ethylcarbodiimide hydrochloride, anhydrous DMF.

CH_2), 4.48 (s, 2H, CH_2), 5.41 (s, 1H, H pyrazole), 6.72 (s, 1H, furyl), 6.82 (d, 1H, H ar, $J = 6.8$ Hz), 6.89–6.94 (m, 2H, ar), 7.05 (s, 1H, furyl), 7.19–7.23 (m, 3H, 1 ar + NH_2, exchangeable with D_2O), 7.36 (s, 1H, NH, exchangeable with D_2O), 7.82–7.91 (m, 5H, 4 ar + 1 furyl).

Anal. Calcd for ($C_{29}H_{26}N_8O_4S$): C, 59.78; H, 4.50; N, 19.23; Found: C, 59.99; H, 4.35; N, 19.57.

2.2. Binding and cAMP assays

Derivative P686 was tested for its affinity at hA1R, hA2AR, and hA3R receptors, stably transfected in Chinese hamster ovary (CHO) cells, using radioligand binding assays. Additionally, the inhibitory effect of P686 on 5'-(N-ethylcarboxamido) adenosine (NECA)-stimulated cAMP levels was measured in hA_{2B} CHO cells. cAMP assays were also performed in hA_{2A} CHO cells to evaluate the antagonistic effect of P686 on NECA-induced cAMP accumulation. These experiments were carried out as previously described (Varano et al., 2016).

2.3. Animals

Wistar rats (Envigo, Italy) were used for the preparation of primary cell cultures. All animal experiments satisfied the regulatory requirements of the European Parliament (Directive, 2010/63/EU), European Union Council (September 22, 2010), and Italian Animal Welfare Law (DL 26/2014). The protocol received approval from the Institutional Animal Care and Use Committee (Univ. Florence) and the Italian Ministry of Health. Animal suffering and the animal number required for data reproducibility were minimized, accordingly with the Ministerial notification (ser. no. 211/2022).

2.4. Cell culture preparations

2.4.1. Purified primary OPC cultures

OPCs were prepared from P1 to P2 rats, as described (Coppi et al., 2020). Briefly, rat pups were sacrificed, and cortices removed, mechanically and enzymatically dissociated, suspended in Dulbecco's Modified Eagle's Medium (DMEM; Euroclone, Italy, #ECB750) containing 100 U/mL penicillin/streptomycin (P/S; Merck, Germany, #P0781), 4 mM L-glutamine (L-Gln; Merck, Germany, #59202C), and 20 % fetal bovine serum (FBS; Merck, Germany, #F7524) and plated in 8.3 mM poly-L-lysine (Merck, Germany, #P4832) coated T75 flasks. After 7 days in culture, microglial cells were removed from the mixed glial cells by a 1 h preshake. OPCs were then separated from glial cultures by 5 h of horizontal shaking. Suspended separated cells were then replaced onto plastic culture dishes for an additional 30 min, to allow adhesion of residual microglial cells. Purified OPCs were suspended in Neurobasal medium (NB; Thermo Fisher, USA, #21103049) supplemented with 2 % B27 (Thermo Fisher, USA, #17504044), 100 U/mL P/S and 4 mM L-Gln and then plated onto 50 μg/mL poly-D,L-ornhitine (Merck Germany, #P8638)-coated surfaces as follows: for patch clamp experiments 10,000 cells per well (24-well plates), for RT-PCR 100,000 cells per well (6-well plates), for DCF assay 20,000 cells per well (24-well plates) and for OPC/DRGN co-cultures 50,000 cells per well (24-well plates), seeded directly onto DRGNs, as described below.

2.4.2. OPC/DRGN cocultures

DRGs were isolated from P5-6 pups as described (Cherchi et al., 2024). Briefly, ganglia were bilaterally removed and dissociated with 2 mg/mL of type 1A collagenase (Merck, Germany, #C9891) and 1 mg/mL of trypsin (Merck, Germany, #T9201) in Hank's balanced salt solution (Merck, Germany, #H8264) at 37 °C for 30 min. Cells were pelleted and subjected to mechanical digestion. Subsequently, they were centrifuged and resuspended in NB medium supplemented with 2 % B27, 100 U/mL P/S and 4 mM L-Gln. Cells were then plated at a density of 15,000 cells per well on 13-mm glass coverslip coated with 8.3 mM poly-L-lysine and 5 mM laminin (Merck, Germany, #L2020). Nerve growth factor (NGF, 100 ng/mL; Thermo Fisher, USA, # A42578) was added to promote neuron survival, while cytosine arabinoside (Ara-C, 10 mM; Merck, Germany, #C1768) was used to remove eventual contaminating fibroblasts and glial cells. Following isolation, DRGNs were maintained in NB medium to permit neurite out-growth for at least one week before OPC seeding. During the final phase of OPC preparation (shaking), NGF was removed from DRGN cultures, as it has been shown to impair OPC differentiation (Chan et al., 2004; Lee et al., 2007; Vaes et al., 2021). Two days before OPC seeding, Ara-C was also removed. Purified OPCs, prepared as described above, were resuspended in the same NB medium and seeded onto DRGNs at a density of 50,000 cells per well. OPC/DRGN cocultures were maintained for 14 days in the presence of the pro-myelinating hormone T3 (50 nM; Merck, Germany, #T6397; Calza et al., 2002). In order to study the effect of $A_{2A}R$ on myelination processes, selective ligands for this receptor subtype were added every 2 days from t3 to t14, considering the time 0 (t0) as the day at which OPCs were added onto DRGNs.

2.5. Electrophysiology

Whole-cell patch-clamp recordings were performed on purified primary OPC cultures as described (Coppi et al., 2020). Cells were transferred to a recording chamber (1 ml volume) mounted on the platform of an inverted microscope (Olympus CKX41, Milan, Italy) and superfused at a flow rate of 1.5 ml/min with a standard extracellular solution containing (mM): HEPES 5, D-glucose 10, NaCl 140, KCl 5.4, $MgCl_2$ 1.2, and $CaCl_2$ 1.8 (pH adjusted to 7.3 with NaOH). In electrophysiological experiments, as specified in each legend, in the presence of the endogenous ligand adenosine, the following adenosine receptor antagonists were added to the extracellular solution: 100 nM DPCPX, 10 nM PSB603 and 100 nM MRS1523, in order to block A_1R, $A_{2B}R$ and A_3R respectively. Borosilicate glass electrodes (Harvard Apparatus, Holliston, Massachusetts USA) were pulled with a Sutter Instruments puller (model P-87) to a final tip resistance of 4–7 MΩ. Standard pipette solution contained (in mM): K-gluconate 130, NaCl 4.8, $MgCl_2$ 2, $CaCl_2$ 1, Na_2-ATP 2, Na_2-GTP 0.3, EGTA 3, HEPES 10 (pH adjusted to 7.4 with KOH). The calculated liquid junction potential (LJP) in these experimental conditions was 14.8 mV and this value was subtracted from all experiments. Data were acquired with an Axopatch 200B amplifier (Axon Instruments, CA, USA), low pass filtered at 10 kHz, stored and analyzed with pClamp 9.2 software (Axon Instruments, CA, USA). All the experiments were carried out at room temperature (RT: 20–22 °C). Protocols. Unless otherwise stated, cells were voltage-clamped at −70 mV. Series resistance (Rs), membrane resistance (Rm) and membrane capacitance (*Cm*) were routinely measured by fast hyperpolarizing voltage pulses (from −70 to −75 mV, 40 ms duration). Only cells showing a stable *Cm* and Rs before, during, and after drug application were included in the analysis. Immediately after seal breaking through, cell resting membrane potential (Vm) was determined by switching to the current-clamp mode. A voltage ramp protocol (800 ms depolarization from −120 to +80 mV) was recorded every 15 s to evoke a wide range of overall voltage-dependent membrane currents before, during and after drug treatments. Variations in membrane potential (Vm) induced by drug treatments were measured by calculating the reversal potential (the "zero current" potential) of ramp-evoked currents before, during and after drug application. Outward K^+ currents were evoked by two different depolarizing voltage-step protocols in order to separate delayed rectifier outward K^+ currents (I_K) from transient outward (I_A) conductances. The first protocol consisted in 10 mV depolarizing voltage steps from −40 to +80 mV (200 ms each, 1 s inter-step interval) preceded by a 100 ms pre-step potential (Vpre) at −80 mV. This protocol activates a mixture of outward I_K and I_A currents in cultured OPCs. Since transient I_A currents present a voltage-dependent inactivation at potential positive to −80 mV, a second protocol was applied in the same cell with a Vpre at −40 mV, to selectively inactivate I_A thus leaving the I_K component unchanged. Net I_A current was then obtained in each cell

by digital subtraction of the two current traces. Current-to-voltage relationships (I-V plots) of I_K or I_A currents were obtained by measuring current amplitude at the steady state (200–250 ms after step onset) of the I_K protocol or at the peak of subtracted trace (1–20 ms after step onset), respectively. Current amplitude (measured as pA) was normalized to respective cell capacitance (*Cm*, measured in pF) and expressed as current density (pA/pF) in averaged results. All drugs were applied by superfusion with a three-way perfusion valve controller (Harvard Apparatus, Holliston, MA USA) after a stable baseline of ramp-evoked currents was obtained. A complete exchange of bath solutions in the recording chamber was achieved within 28 s.

2.6. RNA extraction and quantitative real-time PCR (qRT-PCR) analysis

Total RNA was extracted from OPCs using TriReagent (Sigma-Aldrich) according to the manufacturer's instructions. Briefly, RNA concentration and purity were determined using a NanoDrop 1000 spectrophotometer (Thermo Fisher Scientific). For cDNA synthesis, 500 ng of total RNA was reverse transcribed using the SuperScript™ IV VILO™ Master Mix (Thermo Fisher Scientific). Quantitative real-time PCR was performed on a CFX96 Touch Real-Time PCR Detection System (Bio-Rad) using SYBR Green chemistry (Bio-Rad). Gene expression levels of MAG (qRnoCID0002891), and MBP (qRnoCED0007813) were analyzed, with β-actin (qRnoCID0056984) serving as the internal reference gene. Relative mRNA expression levels were calculated using the $2^{\wedge(-\Delta\Delta Ct)}$ method (Livak and Schmittgen, 2001) employing CFX Maestro software (Bio-Rad).

2.7. ROS detection assay

OPCs were plated on glass coverslips and incubated for 3 h with increasing concentrations of hydrogen peroxide (H_2O_2; 3, 10, 100, and 300 μM), or pretreated with 100 nM P625, 300 nM P686, 100 nM SCH58261, or varying concentrations of edaravone (0.3–10 μM) prior to exposure to H_2O_2 (300 μM). Intracellular reactive oxygen species (ROS) levels were assessed using the fluorescent probe DCF-FITC (5 μM; Thermo Fisher Scientific, #C6827). After incubation with DCF-FITC for 30 min at 37 °C in the dark, cells were washed twice with phosphate-buffered saline (PBS) and fixed with 4 % paraformaldehyde for 20 min at room temperature. Coverslips were then washed with PBS and mounted onto microscope slides using a mounting medium. Fluorescence intensity was analyzed by confocal microscopy in at least eight randomly selected fields per condition. Fluorescence signals were normalized to the total cell number.

2.8. Immunofluorescence

OPC/DRGN cocultures were fixed with 4 % paraformaldehyde in 0.1 M phosphate-buffered saline (PBS, Corning, USA, #21-030-CV) for 10 min at RT. Cells were washed twice with PBS and then incubated in PBS solution containing 0.25 % Triton X-100 (PBST; Merck, Germany, #X100). After three washes in PBS, cells were incubated in blocking buffer (BB, 10 % normal goat serum (GS; Merck, Germany, #G9023) in PBST) for 30 min to block unspecific binding sites. Cells were then incubated for 2.5 h at RT with the appropriate primary antibodies, dissolved in BB. Finally, cells were washed three times with PBS and then incubated 1 h at RT with specific secondary antibodies dissolved in BB. Primary antibodies used: rabbit *anti*-βIII-Tubulin (1:400; Cell Signaling, USA, #D71G9) and mouse anti-myelin basic protein (MBP) (1:500; Cell Signaling, USA, #E9P7U). AlexaFluor 488 donkey anti-rabbit (1:500; Invitrogen, USA, #A21206) and AlexaFluor 555 donkey anti-mouse (1:500; Invitrogen, USA, #A31570) were used as fluorescent secondary antibodies. Coverslip were mounted with Fluoroshield containing DAPI to stain cell nuclei. Control experiments were performed by incubating fixed cells with the secondary antibodies and DAPI to exclude nonspecific signals.

2.9. Confocal microscopy and semi-quantitative analysis

Immunocytochemical images were captured by a Leica SP8 laser scanning confocal microscope (Leica Microsystems, Mannheim, Germany). OPC/DRGN coculture images were acquired with a 20 × /NA 0.75 objective using the following capture setting: 2048 × 2048 pixels, scanning speed of acquisition 200 Hz and z-step of 1 μm. The collected OPC/DRGN images were acquired blind and were analyzed by a different researcher with an open-source software (Fiji-ImageJ, version 1.49v National Institutes of Health, Bethesda, MD, USA; Schneider et al., 2012). MBP immunofluorescence was quantified by the number of positive pixels above a threshold level in each confocal microscopy z-projection of 10 consecutive confocal z-scans (total thickness 10 μm; Gerace et al., 2021) with the threshold tool in 3 random fields per coverslip. In the same images, the Manders' overlap coefficient (M1) was also evaluated: this parameter represents the myelination index, estimated as the fraction of βIII-Tubulin positive pixels overlapping the MBP positive pixels in each region of interest (ROI), by using JACop plugin of ImageJ (Bolte and Cordelières, 2006; Igado et al., 2020). The number of cocultures was represented by the symbol "N," while the number of replications of every single condition was indicated by the lowercase letter "n."

2.10. Drugs

The $A_{2A}R$ agonist 4-[2-[[6-Amino-9-(N-ethyl-β-D-ribofuranuronamidosyl)-9H-purin-2-yl]amino]ethyl]benzenepropanoic acid hydrochloride (CGS21680; Tocris, UK, #1063), the $A_{2A}R$ antagonist 2-(2-Furanyl)-7-(2-phenylethyl)-7H-pyrazolo[4,3-e][1,2,4]triazolo[1,5-c] pyrimidin-5-amine (SCH58261; Tocris, UK, #2270), the A_1R antagonist 8-Cyclopentyl-1,3-dipropylxanthine (DPCPX; Tocris, UK, #0439), the $A_{2B}R$ antagonist 8-[4-[4-(4-Chlorophenzyl)piperazide-1-sulfonyl) phenyl]]-1-propylxanthine (PSB603; Tocris, UK, #3198); the A_3R antagonist 3-Propyl-6-ethyl-5-[(ethylthio)carbonyl]-2 phenyl-4-propyl-3-pyridine carboxylate (MRS1523; Merck, Germany, #M1809), Edaravone (Merck, Germany, #M70800), the endogenus ligand adenosine (Merck, Germany, #A4036) were used. All drugs, including P400, P625 and the novel synthetized P686, were dissolved in dimethyl sulphoxide (DMSO; Merck, Germany, #472301), except for adenosine that was dissolved in distilled water. Stock solutions, of 1000–10,000 times the desired final concentration, were stored at −20 °C. Control experiments demonstrated that the maximal DMSO concentration used in the present work (0.1 %) was inactive in modulating membrane currents in OPCs (data not shown).

2.11. Statistics

Data were evaluated using the Shapiro–Wilk test to confirm the normality of the distribution. All data are presented as mean ± SEM (standard error of the mean). Regarding RT-PCR experiments, data are presented as mean ± SEM from three independent experiments, each performed in triplicate. Two-tailed Student's paired *t*-tests, one-way ANOVA and two-way ANOVA followed by appropriate posthoc test was performed as indicated in the figure legend in order to determine statistical significance ($p < 0.05$). Data were analyzed using GraphPad Prism 8th edition (GraphPad Software, San Diego, CA, USA) software.

3. Results

3.1. Selective $A_{2A}R$ activation inhibited voltage-dependent K^+ currents in cultured OPCs and this effect was prevented by the thiazolopyrimidine $A_{2A}R$ antagonists

Electrophysiological recordings were performed on 125 cells, which showed a resting membrane potential (Vm) of −71.29 ± 2.07 mV, membrane capacitance (*Cm*) of 9.08 ± 0.21 pF, and membrane

resistance (Rm) of 1154 ± 80 MΩ.

As shown in Fig. 2, the selective $A_{2A}R$ agonist CGS21680 (100 nM, 5 min application) reversibly inhibited outward K^+ currents evoked by a voltage ramp protocol (from −120 to +80 mV, 800 ms duration) in cultured OPCs, consistent with previous findings (Coppi et al., 2013). The CGS21680-sensitive current, obtained by subtracting the ramp recorded in the presence of the ligand from the control ramp, revealed a voltage-dependent outward conductance gating at −20 mV (Fig. 2C). Results were confirmed in 24 cells: one-way ANOVA ($F(4, 39) = 10.58$; $p < 0.0001$) followed by Bonferroni's post-hoc test revealed significant effect in preventing CGS21680-inhibition by the canonical $A_{2A}R$ antagonist SCH58261 (100 nM; ***p = 0.0003) and by the thiazolopyrimidine $A_{2A}R$ antagonists P625 and P400 (both 100 nM; **p = 0.0053 and *p = 0.0379, respectively; Fig. 2D).

To confirm these findings, the endogenous ligand adenosine was applied at nanomolar concentration (100 nM) in the presence of selective antagonists for other adenosine receptors expressed in OPCs: DPCPX (A_1R; 100 nM), PSB603 ($A_{2B}R$; 10 nM) and MRS1523 (A_3R; 100 nM). Consistently with results obtained in the presence of the selective $A_{2A}R$ agonist CGS21680, adenosine inhibited outward potassium currents elicited by the voltage ramp protocol in cultured OPCs (Fig. 3A–B). As shown in Fig. 3C, selective $A_{2A}R$ antagonists (SCH58261, P625 and P400) also blocked adenosine inhibitory effect on outward potassium currents. One-way ANOVA performed across all treatment groups, including the newly synthesized compound P686, revealed a significant effect of treatments ($F(4, 45) = 13.20$; $p < 0.0001$). Bonferroni's post-hoc tests showed that adenosine-inhibition was significantly prevented by SCH58261 (****p < 0.0001), P625 (****p < 0.0001) and P400 (**p = 0.0011). In this assay, we tested the effect of the newly synthesized compound P686, an $A_{2A}R$ antagonist hybridized with the free radical scavenger edaravone. The new ligand significantly prevented the inhibition of potassium currents induced by adenosine (****p < 0.0001), confirming that hybridization with edaravone did not interfere with $A_{2A}R$ binding (Fig. 3C).

Binding assays performed on human $A_{2A}R$ revealed a Ki value of 15.1 nM for P625 (Varano et al., 2020a), indicating high affinity for the target. To assess its functional potency in our electrophysiological model, P625 was applied at increasing concentrations (1–100 nM) in the continuous presence of adenosine, and its ability to counteract the adenosine-induced inhibition of ramp-evoked currents was evaluated using whole-cell patch-clamp recordings (Supplementary Fig. 1). P625 reduced the inhibitory effect of adenosine on outward potassium current in a concentration-dependent manner, with an IC_{50} value of 2.30 nM (Fig. 3D).

As previously demonstrated, $A_{2A}R$ activation inhibited delayed rectifier potassium currents (I_K) without affecting transient potassium currents (I_A) (Coppi et al., 2013). Specifically, adenosine significantly reduced I_K currents evoked by a voltage step protocol (from – 40 to +80 mV, Vpre = −40 mV; 200 ms), as assessed by paired *t*-test (n = 12) but had no effect on I_A currents (Fig. 3E–H). Significant differences in current density were observed at different step potentials; full statistical details (t-values, degrees of freedom, and exact p-values) are provided in the supplementary material (Supplementary Table 1).

Since P686 is hybridized with edaravone, which is known to exert effects on OPCs (Mahmoud et al., 2025; Takase et al., 2018a), we conducted another set of experiments to test the impact of edaravone on

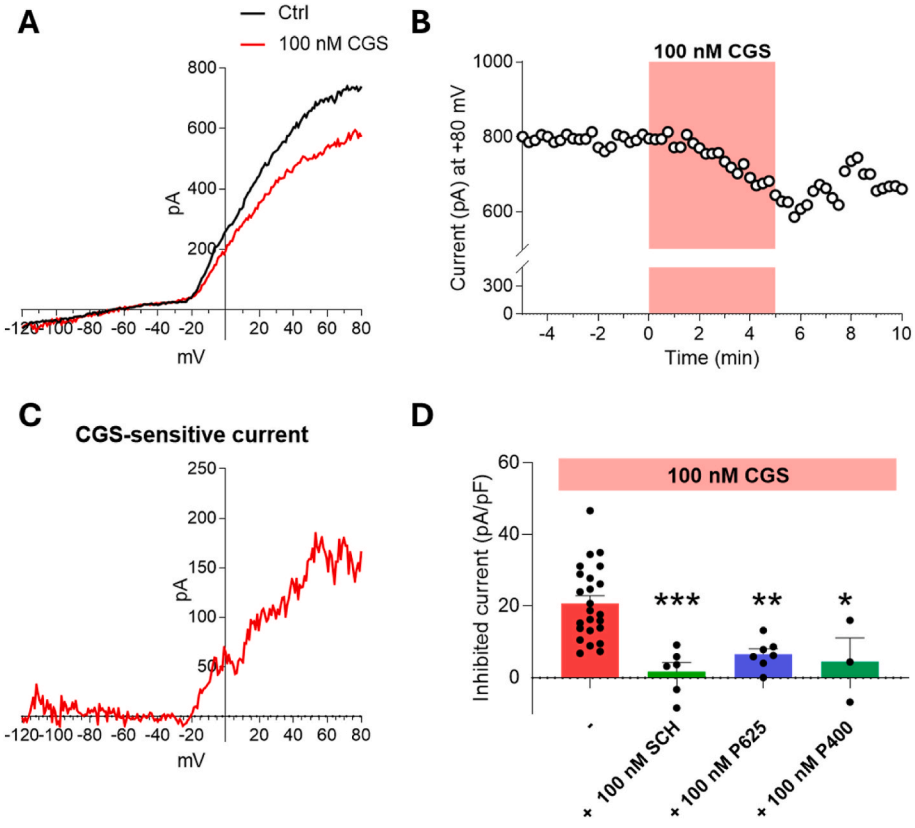

Fig. 2. The selective $A_{2A}R$ agonist CGS21680 inhibits outward potassium currents in cultured OPCs: an effect reversed by the canonical antagonist SCH58261 and by the two thiazolopyrimidine $A_{2A}R$ antagonists, P625 and **P400. A.** Original whole-cell patch clamp current traces evoked by a voltage ramp protocol (from −120 to +80 mV, 800 ms) in a typical OPC before (Ctrl: black trace) or after application of CGS21680 (100 nM CGS: red trace). **B.** Time course of ramp-evoked currents at +80 mV in the same cell. **C.** Net CGS-inhibited current, obtained by subtraction of the trace recorded in CGS from the control ramp, in the same cell. **D.** Pooled data (mean ± SEM) of CGS-induced outward current inhibition obtained in the absence or presence of different $A_{2A}R$ antagonists: SCH58261 (SCH; 100 nM) or P625 (100 nM) or P400 (100 nM) in cultured OPCs. *p < 0.05; **p < 0.01, ***p < 0.001 one-way ANOVA, Bonferroni post-test. (For interpretation of the references to colour in this figure legend, the reader is referred to the Web version of this article.)

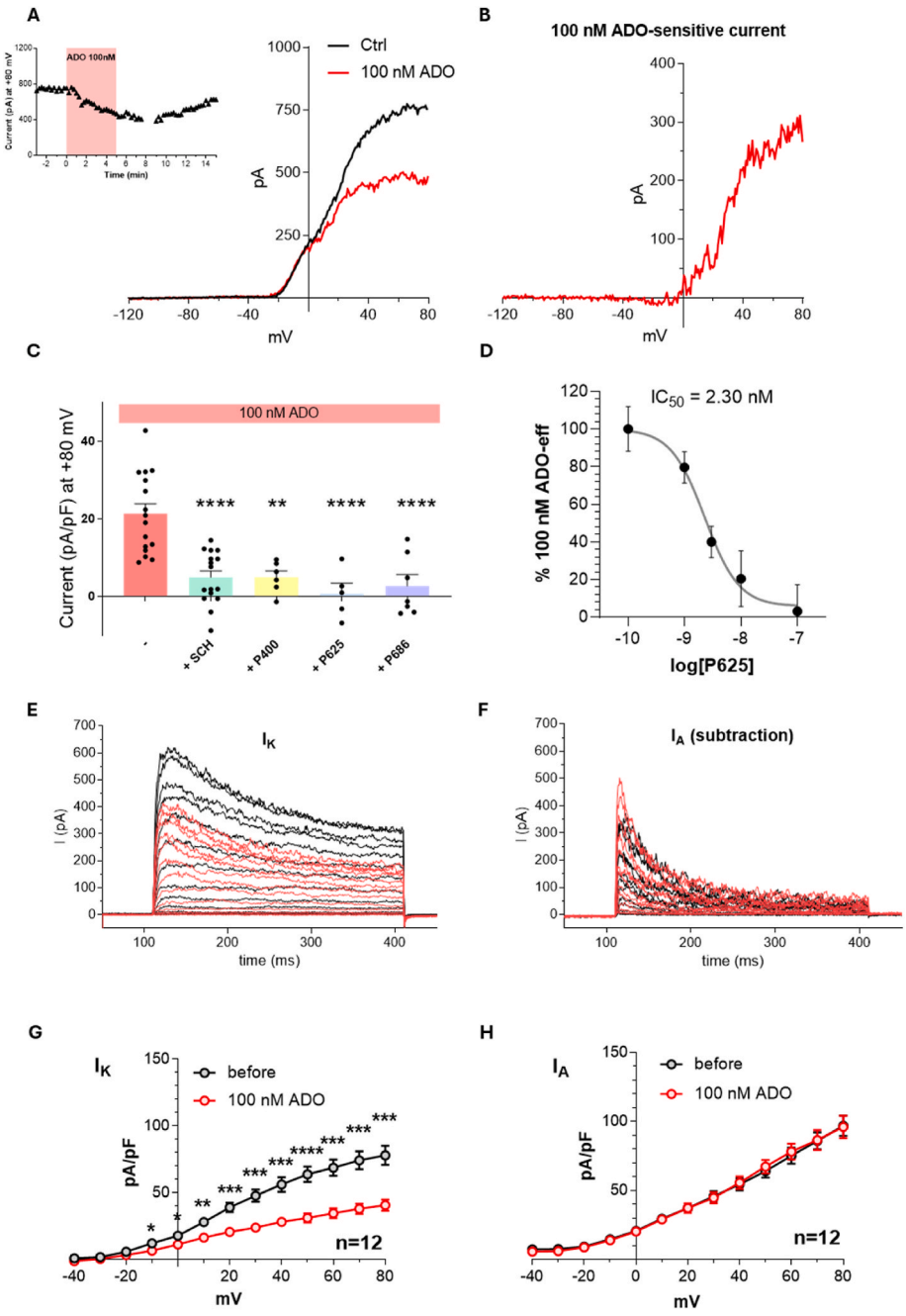

Fig. 3. The endogenous ligand adenosine inhibits delayed rectifier (I_K)outward K^+ currents in cultured OPCs via the activation of A_{2A}Rs and this effect was prevented by the thiazolopyrimidine A_{2A}R antagonists and the novel compound **P686. A.** Original whole-cell patch clamp current traces evoked by a voltage ramp protocol (from −120 to +80 mV, 800 ms) in a typical OPC before (Ctrl: black trace) or after application of adenosine (100 nM ADO: red trace). Inset: Time course of ramp-evoked currents at +80 mV in the same cell. **B.** Net ADO-inhibited current, obtained by subtraction of the trace recorded in adenosine from the control ramp, in the same cell. **C.** Pooled data of ADO-induced ramp-evoked K^+ current inhibition obtained in the absence or presence of different A_{2A}R antagonists: SCH58261 (SCH; 100 nM), P625 (100 nM), P400 (100 nM), or the new edaravone-conjugated hybrid A_{2A}R antagonist P686 (100 nM) in cultured OPCs. **p < 0.01; ****p < 0.0001, one-way ANOVA, Bonferroni post-test. **D.** Concentration–response curve of the effect of P625 (1–100 nM) on ADO inhibition (IC_{50} = 2.26 nM, confidence limits: 0.77–31.5 nM). **E.** Original I_K current traces obtained in the same OPC by a voltage-step protocol (from - 40 to +80 mV, Vpre = −40 mV; 200 ms). **F.** Net I_A current obtained in the same cell by digital subtraction of the traces shown in E (I_K) from those obtained by applying the same protocol but with a Vpre = −80 mV (I_K + I_A). **G-H.** Averaged (mean ± SEM) current-to-voltage relationship (I-V plot) of steady-state sustained, I_K (**G**), or peak, transient, I_A (**H**) recorded in the absence (ctrl: black circles) or in the presence (red circles) of 100 nM ADO in 12 cells investigated. *p < 0.05; **p < 0.01; ***p < 0.001 paired Student's t-test. All experiments were performed in the presence of the A_1R, A_{2B}R and A_3R antagonists: DPCPX (100 nM), PSB603 (10 nM) and MRS1523 (100 nM), respectively. (For interpretation of the references to colour in this figure legend, the reader is referred to the Web version of this article.)

potassium currents. When tested at concentrations of 0.1 and 1 μM, equivalent to the effective concentration of P686, edaravone did not modify outward potassium currents (Supplementary Fig. 2).

3.2. The $A_{2A}R$ antagonists and edaravone-conjugated derivative P686 increased cell differentiation and prevented H_2O_2-induced increase in ROS levels in purified cultured OPCs

The reduction of I_K currents is strictly correlated with a reduction of OPC differentiation in culture (Gallo et al., 1996). In order to permit the differentiation of OPCs to oligodendrocytes, PDGF and FGF were removed from the culture medium for 5 days, as previously demonstrated (Coppi et al., 2013, 2020). Contemporarily, cells were exposed to different $A_{2A}R$ antagonists to assess their effects on oligodendrocyte maturation, by performing quantitative real-time PCR analysis for the expression of myelin-associated gene targets. Both the $A_{2A}R$ antagonist P625 and edaravone-conjugated derivative P686 significantly increased the mRNA levels of MAG and MBP compared to control (Fig. 4), as confirmed by two-way ANOVA showing a significant effect of treatment ($F(7, 67) = 18.06$, $p < 0.0001$ and $F(7, 63) = 3.009$, $p = 0.0086$, respectively). Post-hoc analysis (Dunnett's multiple comparisons test) revealed that only P625 and P686 significantly differed from control for MAG (****$p < 0.0001$ for both compounds) and MBP (*$p = 0.0306$ for P625, and **$p = 0.0042$ for P686) mRNA levels. The other tested compounds, including edaravone, did not induce significant changes in the expression of either gene.

To further evaluate the protective properties of the $A_{2A}R$ antagonists, and the eventual advantage given by edaravone hybridization, we assessed their effects on oxidative stress using the DCF assay. In an initial set of experiments, cells were exposed to increasing concentrations of hydrogen peroxide (H_2O_2: 3–300 μM) for 3 h to boost ROS production (Fig. 5A). Based on these results, which showed a significant increase in ROS level at 300 μM H_2O_2 (one-way ANOVA vs CTRL; $F(4, 14) = 10.29$; $p = 0.0004$; Bonferroni's post-hoc test CTRL vs 300 μM H_2O_2 $^{###}p = 0.003$), subsequent experiments were conducted in which OPCs were pre-treated for 3 h with the tested compounds prior to a 3-h exposure to 300 μM H_2O_2. Under these conditions, all tested compounds prevented H_2O_2-induced increase in ROS levels, as shown by a two-way ANOVA vs H_2O_2 revealing a significant effect of treatments (Column Factor: $F(6, 112) = 18.02$, $p < 0.0001$) and a significant interaction with experimental replicates (Interaction: $F(12, 112) = 8.395$, $p < 0.0001$). Post-hoc analysis (Dunnett's multiple comparison test) confirmed that all compounds significantly prevented the increase in ROS levels (****$p < 0.0001$ for all drugs used). Notably, pre-treatment with compounds containing only the $A_{2A}R$ antagonist core, included SCH58261, also conferred significant protection against H_2O_2-induced ROS elevation, suggesting intrinsic antioxidant properties of SCH58261, as previously demonstrated in other cell types (Sun et al., 2024; Thakur et al., 2010) (Fig. 5B).

3.3. The edaravone-conjugated derivative P686 increased myelination in DRGN/OPC co-cultures

Finally, we evaluated the effects of the tested compounds in OPC/DRGN co-cultures, a well-established in vitro model of myelination. As previously described (Cherchi et al., 2024), oligodendrocyte differentiation is quantified by measuring total MBP expression via immunofluorescence, while myelination is quantified by the Mander's coefficient (M1), which reflects the overlap between MBP^+-pixels and the neuronal marker $\beta III\text{-tubulin}^+$-pixels (Fig. 6). Nested one-way ANOVA revealed a significant effect of treatment on M1 expression ($F(5,12) = 3.167$; $p = 0.0473$), accounting for repeated measures within cocultures. No significant variation was detected within subcolumns ($p > 0.9999$), supporting the reliability of within-animal replicates. As shown in Fig. 6C, only the hybrid compound P686 induced a significant increase in myelination, as evidenced by a higher M1 coefficient (Dunnet's post-hoc test; $p = 0.0254$). These results suggest that the conjugation of an $A_{2A}R$ antagonist with edaravone may enhance myelination more effectively than either agent alone, possibly by simultaneously targeting receptor signalling and oxidative stress pathways.

4. Discussion

Pharmacological strategies able to stimulate OPC differentiation are provide insights into mechanism controlling myelination (Cherchi et al., 2021a). This study aimed to assess the effects of different selective $A_{2A}R$ antagonists and the edaravone-conjugated derivative P686, on OPC differentiation, oxidative stress response and myelination processes. Our results reveal that the compounds facilitate OPC differentiation and reduce the damage produced by oxidative stress. Among the compounds tested, we found that only the edaravone-conjugated derivative P686 promotes myelination of DRGNs cocultured with OPCs, suggesting that edaravone conjugation confers additional neuroprotective and pro-myelinating properties to the $A_{2A}R$ antagonist core.

Electrophysiological experiments performed on OPC cultures confirmed that $A_{2A}R$ activation via CGS21680 and, for the first time, by endogenous neuromodulator adenosine, inhibits voltage-dependent outward potassium currents, particularly the delayed rectifier component (I_K), which is essential for their differentiation (Coppi et al., 2013; Gallo et al., 1996). This inhibitory effect was prevented by the canonical $A_{2A}R$ antagonist SCH58261 or by the novel synthesized antagonists P625 and P400, which also displayed nanomolar potency and high

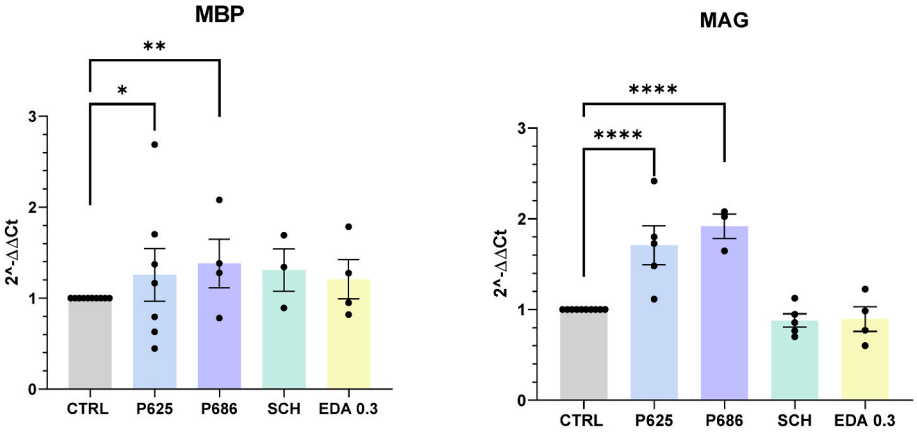

Fig. 4. The edaravone-hybrid derivative P686 increases oligodendrocyte differentiation **in vitro.** Gene expression analysis of oligodendrocyte differentiation markers MAG and MBP by Real Time-PCR (RT-PCR) in OPC differentiated for 5 days in different experimental conditions. RT-PCR was performed by using SYBR green probe and specific rat primers, as reported in methods section. The $2^{(-\Delta\Delta CT)}$ method was employed as a comparative method of quantification and data were normalized to β-actin expression. Data are means ± SEM of three independent experiments performed in triplicate. *$p < 0.05$; **$p < 0.01$; ****$p < 0.0001$, two-way ANOVA, Dunnett's post-test. (For interpretation of the references to colour in this figure legend, the reader is referred to the Web version of this article.)

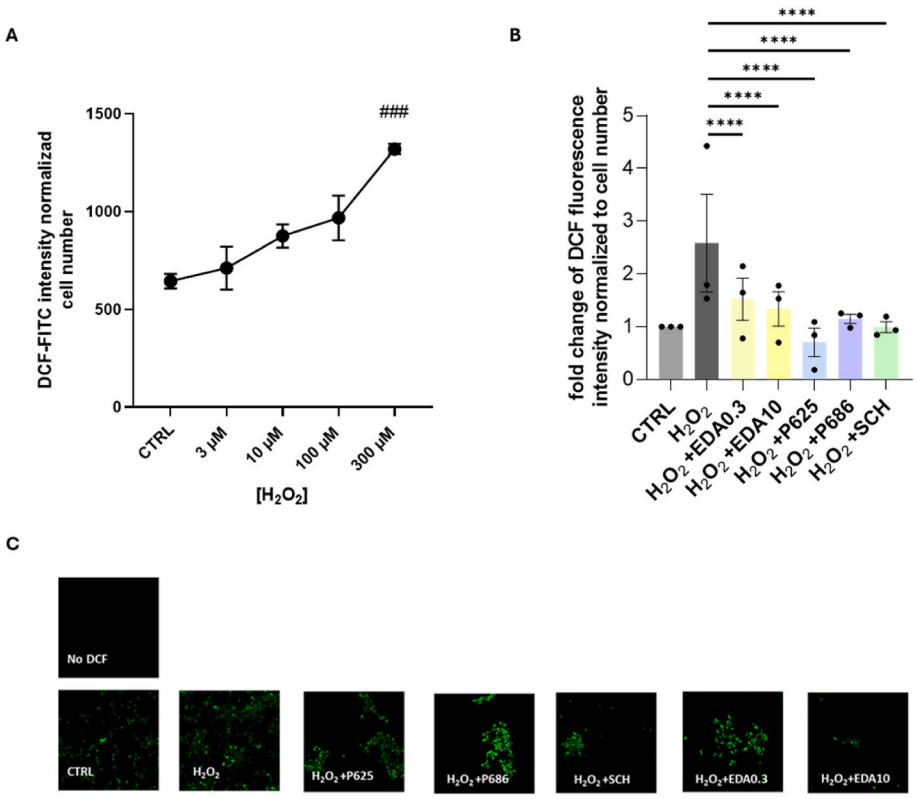

Fig. 5. Antioxidant effect of edaravone, $A_{2A}R$ antagonist and hybrid counterpart P686, in cultured **OPCs. A.** Concentration–response curve of hydrogen peroxide (H_2O_2) effect on ROS production in OPCs based on DCF-FITC fluorescence analysis by confocal microscopy. OPCs were plated in glass microscope coverslip and incubated for 3 h in the absence or in the presence of different concentrations of hydrogen peroxide (3-10-100-300 μM). DCF-FITC was incubated as described in the Methods. **B.** OPCs were plated in glass microscope coverslip and incubated for 3 h with 100 nM P625, 300 nM P686, 100 nM SCH58261 or different concentration of edaravone (0.3–10 μM) before being incubated with H_2O_2 (300 μM, 3 h). Fluorescence intensity was analyzed employing confocal microscopy in at least 8 fields per condition after normalization to total cell number. Data reported in panel A are means ± SEM of three independent experiments performed in triplicate. ###$p < 0.001$ one-way ANOVA Bonferroni post-test. Data reported in panel B are means ± SEM of three independent experiments performed in triplicate. ****$p < 0.0001$, two-way ANOVA, Bonferroni post-test. **C.** Representative confocal images are reported.

functional efficacy. These findings are consistent with previous reports linking $A_{2A}R$ activation to a block in OPC maturation via modulation of potassium currents (Coppi et al., 2013).

Moreover, also the new $A_{2A}R$ antagonist, P686, conjugated with edaravone, prevents the inhibitory effects induced by adenosine, highlighting that the linkage with edaravone does not affect the ability to prevent an A_{2A} -mediated effect on potassium currents. Edaravone, *per se,* does not modify the amplitude of these currents, when applied at concentrations equivalent to those present in the hybrid compound.

Edaravone, a free radical scavenger able to cross the blood brain barrier, is a FDA-approved neuroprotective drug clinically used for the treatment of stroke (Japan) and ASL (USA). The compound has been indicated as a promising drug efficacious for several neurodegenerative diseases and presents a good tolerability (Agresti et al., 2019).

In this study, oligodendrocyte differentiation was assessed by analyzing the expression of two canonical myelin genes, MAG and MBP. MAG expression increases progressively during oligodendrocyte maturation, being absent in OPCs and reaching high levels in mature cells, whereas MBP synthesis coincides with the onset of myelination and is considered a late-stage differentiation marker (Zurbriggen et al., 1984; Xie et al., 2010). As in our previous work (Coppi et al., 2020), we took advantage of the complementary regulation of these two myelin-related genes to provide a reliable quantification of oligodendrocyte progression. By applying the same validated strategy used in that study, we could strengthen the robustness of our analysis, and the consistent upregulation of MAG and MBP in our model offers solid evidence of a pro-differentiating effect of tested compounds. P625 and P686 induce an increase in OPC maturation, as indicated by the increased in MBP and MAG levels found after 5 days of pharmacological treatment. Mature, differentiated OLs are characterized by the production of myelin-related proteins such as MBP and MAG, which are expressed on the cytoplasmic surface of the plasma membrane and myelin associated glycoprotein (MAG) (Simons and Trajkovic, 2006). The increase in OPC differentiation induced by $A_{2A}R$ antagonists indicates a physiological role of adenosine in this process. This suggests that in our in vitro model there might be an endogenous release of adenosine able to activate high affinity $A_{2A}Rs$ which may disclose the antagonist effect.

Many drugs present neuroprotection in different experimental models of pathologies by improving the endogenous antioxidant system and reducing lipid peroxidation to relieve oxidative stress (Forman and Zhang, 2021). We demonstrated that edaravone and the $A_{2A}R$ antagonists, also including the conjugated derivative P686, significantly counteract the increase in ROS levels, as indicated by the increased DCF-fluorescence, induced by the application of micromolar concentrations of H_2O_2. It is well established that the antioxidant edaravone was able to prevent ROS production and to preserve oligodendrocyte function after cerebral hypoperfusion damage in mice (Miyamoto et al., 2013; Takase et al., 2018b; Ueno et al., 2009). Notably, it is described that also the $A_{2A}R$ antagonist SCH58261 alleviates oxidative stress restoring superoxide dismutase activity and glutathione (GSH) content in the cortex in Alzheimer's Disease mice model by promoting the translocation of Nrf2 into the nucleus (Sun et al., 2024) and also in endothelial peripheral cells (Thakur et al., 2010). The protective effects of the compounds against oxidative stress, as shown by their ability to reduce ROS accumulation after H_2O_2 exposure, reinforce the hypothesis that $A_{2A}R$ antagonists themselves possess intrinsic antioxidant activity

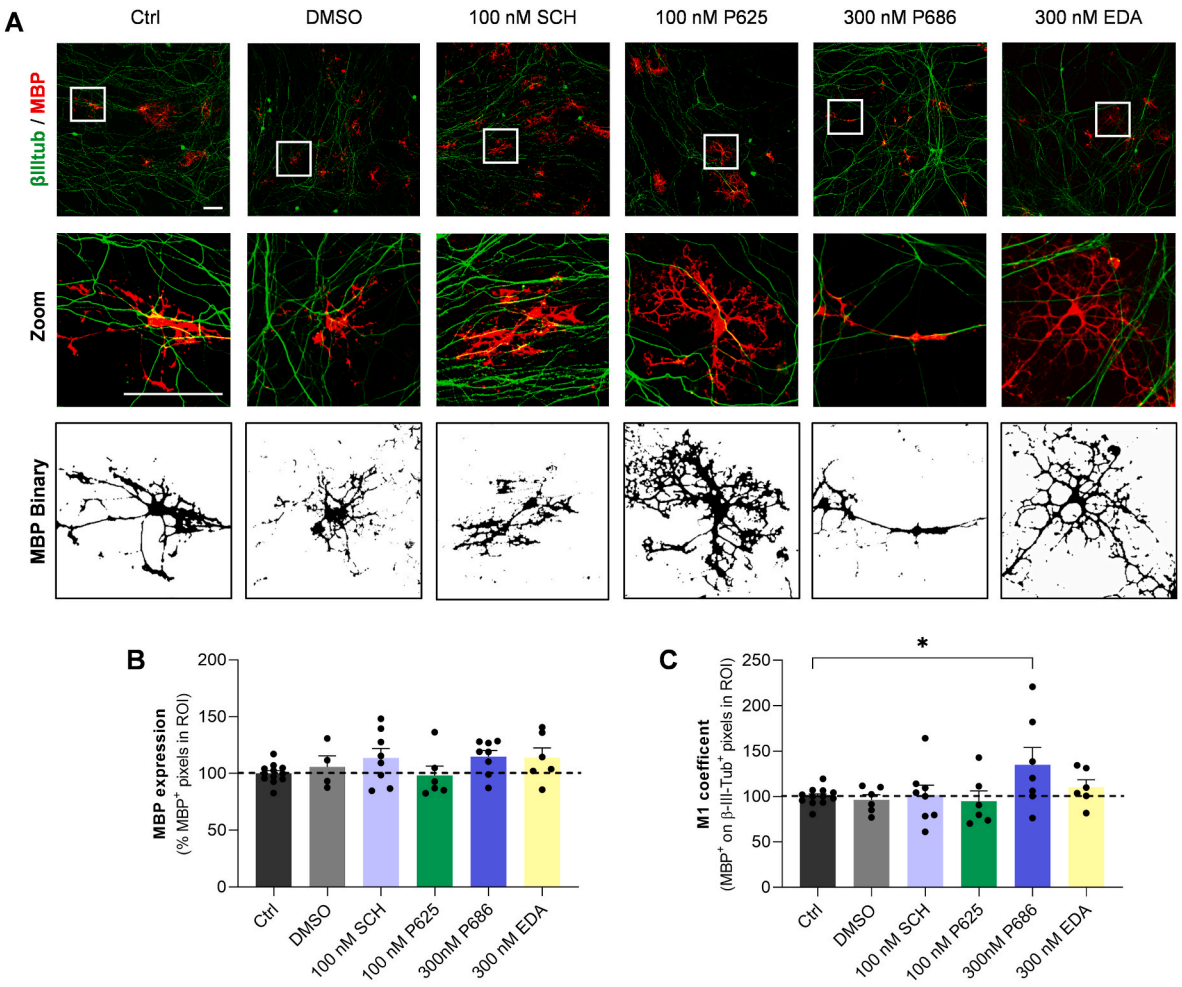

Fig. 6. Only the new synthetized edaravone-conjugated derivative P686 increases myelination in OPC/DRGN co-cultures. **A.** Upper panels: Representative images of OPC/DRGN cocultures stained for myelin basic protein (MBP, red) and βIII-tubulin (green) in different experimental conditions. Magnification: 20X. Scale bar = 50 μm. Middle panels: Magnification of the region of interest (ROI) indicated in the upper panels, to better visualize overlapping between MBP and βIII-tubulin, representing the contact between the oligodendrocyte and the DRG axon. Lower panels: MBP^+ images are converted into binary images to better clarify the oligodendrocyte morphology of the region of interest (ROI) indicated in upper panels. Scale bar = 25 μm. **B-C.** Quantification of MBP (**B**) expression in different experimental conditions at t14: control (CTRL), vehicle (DMSO), SCH58261 (100 nM SCH), P625 (100 nM), P686 (300 nM) and edaravone (300 nM EDA). MBP are reported as percentage change to CTRL at t14. Mander's coefficient (M1 coefficient, **C**) quantified as the overlap of MBP^+ pixels on $βIII\text{-}tubulin^+$ pixels, is reported as percentage change to CTRL at t14 in the same experimental conditions. Data are expressed as mean ± SEM. *$p < 0.05$, Nested One-way ANOVA; Dunnet's post-test vs CTRL group. (For interpretation of the references to colour in this figure legend, the reader is referred to the Web version of this article.)

in vitro. While this effect has been described in non-glial cells (Sun et al., 2024; Thakur et al., 2010), our study is among the first to demonstrate such activity in OPCs.

Since OPC monocultures does not represent a myelination model for the absence of neuronal axons (Marangon et al., 2021), we decided to investigate the role of these compounds, including the antioxidant edaravone, during myelination in OPC/DRGN cocultures. Crucially, in this in vitro model, only P686 was able to significantly increase the M1 coefficient, reflecting enhanced myelination. Although all antagonists promoted OPC differentiation, the addition of edaravone appears necessary to support full maturation into myelinating oligodendrocytes. Our findings provide mechanistic insights into how dual modulation of A_{2A} signalling and oxidative stress can influence oligodendrocyte differentiation and myelination, supporting the idea that targeting multiple pathological pathways can yield synergistic or additive effects on myelination, as suggested in other models of demyelinating disease (Bernardo et al., 2009; Luo et al., 2023).

5. Conclusions

Together, these results provide mechanistic insights into OPC differentiation and myelination in vitro, and support further investigation of dual-target compounds in preclinical models of demyelination While $A_{2A}R$ antagonists alone are promising candidates to promote OPC maturation, their conjugation with antioxidant edaravone, appears to further support myelination-related processes. Future studies should aim to validate these findings in vivo and further elucidate the molecular mechanisms underlying the dual activity of hybrid compounds like P686.

CRediT authorship contribution statement

F. Cherchi: Writing – review & editing, Writing – original draft, Visualization, Supervision, Methodology, Investigation, Data curation, Conceptualization. **L. Frulloni:** Methodology, Investigation, Data curation. **M. Venturini:** Methodology, Investigation, Data curation. **G. Magni:** Methodology, Formal analysis. **S. Calenda:** Methodology. **R. Innocenti:** Conceptualization. **F. Varano:** Methodology, Data curation,

Conceptualization. **D. Catarzi:** Methodology, Data curation, Conceptualization. **C. Ceni:** Methodology. **G. Vagnoni:** Methodology. **V. Colotta:** Supervision, Resources, Methodology, Funding acquisition. **F. Vincenzi:** Methodology, Data curation. **K. Varani:** Supervision, Methodology. **M. Prisinzano:** Methodology. **C. Donati:** Supervision. **F. Cencetti:** Supervision, Methodology, Data curation, Conceptualization. **E. Coppi:** Writing – review & editing, Supervision, Funding acquisition, Data curation, Conceptualization. **A.M. Pugliese:** Writing – review & editing, Supervision, Resources, Funding acquisition, Data curation, Conceptualization.

Declaration of interests and generative AI in scientific writing

All the authors have read and approved the final version submitted, and there are no conflicts of interest involved in this submission. No AI writing in scientific writing upon submission of the paper.

Fundings

The research was funded by the Università degli Studi di Firenze (RICATEN; AMP); by Next Generation European Union, in the context of the National Recovery and Resilience Plan, M4C2 Investment 1.5 (THE - Tuscany Health Ecosystem), CUP B83C22003920001 (AMP, VC and CD); by Next Generation European Union, in the context of the National Recovery and Resilience Plan, M4C2 Investment 1.4 (CN00000041 CN3 "National Center for Gene Therapy and Drugs based on RNA Technology" Spoke #3), CUP B13C22001010001 (AMP) and Supported by FISM (Fondazione Italiana Sclerosi Multipla) cod. 2024/R-Single/038 and financed or co-financed with the '5per mille' public founding (EC).

Declaration of competing interest

The authors declare that they have no known competing financial interests or personal relationships that could have appeared to influence the work reported in this paper.

Acknowledgement

Confocal microscopy acquisitions were carried out at the Cnr—Istituto di Fisica Applicata "Nello Carrara," (Florence, Italy). We specially appreciated the great assistance from the Dr. Francesca Rossi.

Appendix A. Supplementary data

Supplementary data to this article can be found online at https://doi.org/10.1016/j.neuropharm.2025.110724.

References

Adebiyi, O.E., Bynoe, M.S., 2023. Roles of adenosine receptor (subtypes A1 and A2A) in cuprizone-induced hippocampal demyelination. Mol. Neurobiol. 60, 5878–5890. https://doi.org/10.1007/S12035-023-03440-6/FIGURES/8.

Agresti, C., Mechelli, R., Olla, S., Veroni, C., Eleuteri, C., Ristori, G., Salvetti, M., 2019. Oxidative status in multiple sclerosis and off-targets of antioxidants: the case of edaravone. Curr. Med. Chem. 27, 2095–2105. https://doi.org/10.2174/0929867326666190124122752/CITE/REFWORKS.

Amirshahrokhi, K., Imani, M., 2025. Edaravone reduces brain injury in hepatic encephalopathy by upregulation of Nrf2/HO-1 and inhibition of NF-κB, iNOS/NO and inflammatory cytokines. Mol. Biol. Rep. 52. https://doi.org/10.1007/S11033-025-10343-3.

Antonioli, L., Blandizzi, C., Pacher, P., Haskó, G., 2013. Immunity, inflammation and cancer: a leading role for adenosine. Nat. Rev. Cancer. https://doi.org/10.1038/nrc3613.

Bakhtiari, M., Ghasemi, N., Salehi, H., Amirpour, N., Kazemi, M., Mardani, M., 2021. Evaluation of edaravone effects on the differentiation of human adipose derived stem cells into oligodendrocyte cells in multiple sclerosis disease in rats. Life Sci. 282. https://doi.org/10.1016/j.lfs.2021.119812.

Bernardo, A., Bianchi, D., Magnaghi, V., Minghetti, L., 2009. Peroxisome proliferator-activated receptor-γ agonists promote differentiation and antioxidant defenses of oligodendrocyte progenitor cells. J. Neuropathol. Exp. Neurol. 68, 797–808. https://doi.org/10.1097/NEN.0B013E3181ABA2C1.

Bolte, S., Cordelières, F.P., 2006. A guided tour into subcellular colocalization analysis in light microscopy. J. Microsc. 224, 213–232. https://pubmed.ncbi.nlm.nih.gov/17210054/.

Calza, L., Fernandez, M., Giuliani, A., Aloe, L., Giardino, L., 2002. Thyroid hormone activates oligodendrocyte precursors and increases a myelin-forming protein and NGF content in the spinal cord during experimental allergic encephalomyelitis. Proc. Nat. Acad. Sci. United States of America 99, 3258–3263. https://doi.org/10.1073/pnas.052704499.

Chan, J.R., Watkins, T.A., Cosgaya, J.M., Zhang, C., Chen, L., Reichardt, L.F., Shooter, E. M., Barres, B.A., 2004. NGF controls axonal receptivity to myelination by Schwann cells or oligodendrocytes. Neuron 43, 183–191. https://pubmed.ncbi.nlm.nih.gov/15260955/.

Chen, Y., Zhang, Z.X., Zheng, L.P., Wang, L., Liu, Y.F., Yin, W.Y., Chen, Y.Y., Wang, X.S., Hou, S.T., Chen, J.F., Zheng, R.Y., 2019. The adenosine A2A receptor antagonist SCH58261 reduces macrophage/microglia activation and protects against experimental autoimmune encephalomyelitis in mice. Neurochem. Int. 129, 104490. https://doi.org/10.1016/j.neuint.2019.104490.

Cherchi, F., Bulli, I., Venturini, M., Pugliese, A.M., Coppi, E., 2021a. Ion channels as new attractive targets to improve re-myelination processes in the brain. Int. J. Mol. Sci. https://doi.org/10.3390/ijms22147277.

Cherchi, F., Pugliese, A.A.M., Coppi, E., 2021b. Oligodendrocyte precursor cell maturation: role of adenosine receptors. Neural Regen Res 16, 1686. https://doi.org/10.4103/1673-5374.306058.

Cherchi, F., Venturini, M., Magni, G., Frulloni, L., Chieca, M., Buonvicino, D., Santalmasi, C., Rossi, F., De Logu, F., Coppi, E., Pugliese, A.M., 2024. Adenosine A2B receptors differently modulate oligodendrogliogenesis and myelination depending on their cellular localization. Glia 72. https://doi.org/10.1002/GLIA.24593.

Coppi, E., Cellai, L., Maraula, G., Pugliese, A.M., Pedata, F., 2013. Adenosine A2A receptors inhibit delayed rectifier potassium currents and cell differentiation in primary purified oligodendrocyte cultures. Neuropharmacology 73, 301–310. https://doi.org/10.1016/j.neuropharm.2013.05.035.

Coppi, E., Cherchi, F., Fusco, I., Dettori, I., Gaviano, L., Magni, G., Catarzi, D., Colotta, V., Varano, F., Rossi, F., Bernacchioni, C., Donati, C., Bruni, P., Pedata, F., Cencetti, F., Pugliese, A.M., 2020. Adenosine A2B receptors inhibit K+ currents and cell differentiation in cultured oligodendrocyte precursor cells and modulate sphingosine-1-phosphate signaling pathway. Biochem. Pharmacol. 177. https://doi.org/10.1016/j.bcp.2020.113956.

Eleuteri, C., Olla, S., Veroni, C., Umeton, R., Mechelli, R., Romano, S., Buscarinu, M.C., Ferrari, F., Calò, G., Ristori, G., Salvetti, M., Agresti, C., 2017. A staged screening of registered drugs highlights remyelinating drug candidates for clinical trials. Sci. Rep. 7. https://doi.org/10.1038/SREP45780.

Fields, R.D., 2004. Volume transmission in activity-dependent regulation of myelinating glia. Neurochem. Int. 45, 503–509. https://doi.org/10.1016/j.neuint.2003.11.015.

Forman, H.J., Zhang, H., 2021. Targeting oxidative stress in disease: promise and limitations of antioxidant therapy. Nat. Rev. Drug Discov. 20 (9 20), 689–709. https://doi.org/10.1038/s41573-021-00233-1, 2021.

Gallo, V., Zhou, J.M., McBain, C.J., Wright, P., Knutson, P.L., Armstrong, R.C., 1996. Oligodendrocyte progenitor cell proliferation and lineage progression are regulated by glutamate receptor-mediated K+ channel block. J. Neurosci. 16, 2659–2670. https://doi.org/10.1523/jneurosci.16-08-02659.1996.

Gavande, N.S., VanderVere-Carozza, P., Mishra, A.K., Vernon, T.L., Pawelczak, K.S., Turchi, J.J., 2017. Design and structure-guided development of novel inhibitors of the xeroderma pigmentosum group A (XPA) protein-DNA interaction. J. Med. Chem. 60 (19), 8055–8070. https://doi.org/10.1021/acs.jmedchem.7b00780.

Gerace, E., Ilari, A., Caffino, L., Buonvicino, D., Lana, D., Ugolini, F., Resta, F., Nosi, D., Grazia Giovannini, M., Ciccocioppo, R., Fumagalli, F., Pellegrini-Giampietro, D.E., Masi, A., Mannaioni, G., 2021. Ethanol neurotoxicity is mediated by changes in expression, surface localization and functional properties of glutamate AMPA receptors. J. Neurochem. 157, 2106–2118. https://doi.org/10.1111/jnc.15223.

Igado, O.O., Andrioli, A., Azeez, I.A., Girolamo, F., Errede, M., Aina, O.O., Glaser, J., Holzgrabe, U., Bentivoglio, M., Olopade, J.O., 2020. The ameliorative effects of a phenolic derivative of Moringa oleifera leave against vanadium-induced neurotoxicity in mice. IBRO Neurosci. Rep. 9, 164–182. https://doi.org/10.1016/j.ibror.2020.07.004.

Ingwersen, J., Wingerath, B., Graf, J., Lepka, K., Hofrichter, M., Schröter, F., Wedekind, F., Bauer, A., Schrader, J., Hartung, H.-P.P., Prozorovski, T., Aktas, O., 2016. Dual roles of the adenosine A2a receptor in autoimmune neuroinflammation. J. Neuroinflammation 13, 48. https://doi.org/10.1186/s12974-016-0512-z.

Jangra, A., Kwatra, M., Singh, T., Pant, R., Kushwah, P., Ahmed, S., Dwivedi, D., Saroha, B., Lahkar, M., 2016. Edaravone alleviates cisplatin-induced neurobehavioral deficits via modulation of oxidative stress and inflammatory mediators in the rat hippocampus. Eur. J. Pharmacol. 791, 51–61. https://doi.org/10.1016/j.ejphar.2016.08.003.

Lee, X., Yang, Z., Shao, Z., Rosenberg, S.S., Levesque, M., Pepinsky, R.B., Qiu, M., Miller, R.H., Chan, J.R., Mi, S., 2007. NGF regulates the expression of axonal LINGO-1 to inhibit oligodendrocyte differentiation and myelination. J. Neurosci. 27, 220–225. https://www.jneurosci.org/content/27/1/220.

Livak, K.J., Schmittgen, T.D., 2001. Analysis of relative gene expression data using real-time quantitative PCR and the 2−ΔΔCT method. Methods 25, 402–408. https://doi.org/10.1006/METH.2001.1262.

Luo, W., Xu, H., Xu, L., Jiang, W., Chen, C., Chang, Y., Liu, C., Tian, Z., Qiu, X., Xie, C., Li, X., Chen, H., Lai, S., Wu, L., Cui, Y., Tang, C., Qiu, W., 2023. Remyelination in neuromyelitis optica spectrum disorder is promoted by edaravone through mTORC1 signaling activation. Glia 71, 284–304. https://doi.org/10.1002/GLIA.24271.

Mahmoud, A.M.A., Helal, M.G., El-Sherbiny, M., Said, E., Nader, M.A., Shehatou, G.S.G., 2025. Edaravone protects against cuprizone-induced demyelination in rats by

modulating TNF-α/NF-κB/NLRP3 signaling and the kynurenine pathway. Eur. J. Pharmacol. 999, 177686. https://doi.org/10.1016/J.EJPHAR.2025.177686.
Marangon, D., Caporale, N., Boccazzi, M., Abbracchio, M.P., Testa, G., Lecca, D., 2021. Novel in vitro experimental approaches to study myelination and remyelination in the central nervous system. Front. Cell. Neurosci. 15. https://doi.org/10.3389/FNCEL.2021.748849.
Miller, E., Wachowicz, B., 2013. Advances in antioxidative therapy of multiple sclerosis. Curr. Med. Chem. 20, 4720–4730. https://doi.org/10.2174/09298673113209990156.
Mills, J.H., Alabanza, L.M., Mahamed, D.A., Bynoe, M.S., 2012. Extracellular adenosine signaling induces CX3CL1 expression in the brain to promote experimental autoimmune encephalomyelitis. J. Neuroinflammation 9. https://doi.org/10.1186/1742-2094-9-193.
Miyamoto, N., Maki, T., Pham, L.D.D., Hayakawa, K., Seo, J.H., Mandeville, E.T., Mandeville, J.B., Kim, K.W., Lo, E.H., Arai, K., 2013. Oxidative stress interferes with white matter renewal after prolonged cerebral hypoperfusion in mice. Stroke; a journal of cerebral circulation 44, 3516. https://doi.org/10.1161/STROKEAHA.113.002813.
Otomo, E., Tohgi, H., Kogure, K., Hirai, S., Takakura, K., Terashi, A., Gotoh, F., Maruyama, S., Tazaki, Y., Shinohara, Y., Ito, E., Sawada, T., Yamaguchi, T., Kikuchi, H., Kobayashi, S., Fujishima, M., Nakashima, M., 2003. Effect of a novel free radical scavenger, edaravone (MCI-186), on acute brain infarction: randomized, placebo-controlled, double-blind study at multicenters. Cerebrovasc. Dis. 15, 222–229. https://doi.org/10.1159/000069318.
Rissanen, E., Virta, J.R., Paavilainen, T., Tuisku, J., Helin, S., Luoto, P., Parkkola, R., Rinne, J.O., Airas, L., 2013. Adenosine A2A receptors in secondary progressive multiple sclerosis: a [11 C]TMSX brain PET study. J. Cerebr. Blood Flow Metabol. 33, 1394–1401. https://doi.org/10.1038/jcbfm.2013.85.
Schneider, C.A., Rasband, W.S., Eliceiri, K.W., 2012. NIH image to ImageJ: 25 years of image analysis. Nat. Methods 9, 671–675. https://www.nature.com/articles/nmeth.2089.
Simons, M., Trajkovic, K., 2006. Neuron-glia communication in the control of oligodendrocyte function and myelin biogenesis. J. Cell Sci. 119, 4381–4389. https://doi.org/10.1242/JCS.03242.
Spaas, J., van Veggel, L., Schepers, M., Tiane, A., van Horssen, J., Wilson, D.M., Moya, P. R., Piccart, E., Hellings, N., Eijnde, B.O., Derave, W., Schreiber, R., Vanmierlo, T., 2021. Oxidative stress and impaired oligodendrocyte precursor cell differentiation in neurological disorders. Cell. Mol. Life Sci. 78 (10 78), 4615–4637. https://doi.org/10.1007/S00018-021-03802-0, 2021.
Stevens, B., Porta, S., Haak, L.L., Gallo, V., Fields, R.D., 2002. Adenosine: a neuron-glial transmitter promoting myelination in the CNS in response to action potentials. Neuron 36, 855–868. https://doi.org/10.1016/S0896-6273(02)01067-X.
Sun, Y., Liu, C., He, L., 2024. Adenosine A2A receptor antagonist Sch58261 improves the cognitive function in alzheimer's disease model mice through activation of Nrf2 via an autophagy-dependent pathway. Antioxidants Redox Signal. https://doi.org/10.1089/ARS.2023.0455/ASSET/IMAGES/ARS.2023.0455_FIGURE6.JPG.
Takase, H., Liang, A.C., Miyamoto, N., Hamanaka, G., Ohtomo, R., Maki, T., Pham, L.D. D., Lok, J., Lo, E.H., Arai, K., 2018a. Protective effects of a radical scavenger edaravone on oligodendrocyte precursor cells against oxidative stress. Neurosci. Lett. 668, 120–125. https://doi.org/10.1016/J.NEULET.2018.01.018.
Takase, H., Lok, J., Arai, K., 2018b. A radical scavenger edaravone and oligodendrocyte protection/regeneration. Neural Regen Res 13, 1550. https://doi.org/10.4103/1673-5374.237116.
Thakur, S., Du, J., Hourani, S., Ledent, C., Li, J.M., 2010. Inactivation of adenosine A2A receptor attenuates basal and angiotensin II-induced ROS production by Nox2 in endothelial cells. J. Biol. Chem. 285, 40104–40113. https://doi.org/10.1074/jbc.M110.184606.
Ueno, Y., Zhang, N., Miyamoto, N., Tanaka, R., Hattori, N., Urabe, T., 2009. Edaravone attenuates white matter lesions through endothelial protection in a rat chronic hypoperfusion model. Neuroscience 162, 317–327. https://doi.org/10.1016/J.NEUROSCIENCE.2009.04.065.
U.S. Food and Drug Administration, 2022. FDA approves oral form of edaravone for treatment of ALS [Online]. Available at: https://www.fda.gov/drugs/news-events-human-drugs/fda-approves-oral-form-treatment-adults-amyotrophic-lateral-sclerosis-als (Accessed: 19 October 2025).
Varano, F., Catarzi, D., Vincenzi, F., Betti, M., Falsini, M., Ravani, A., Borea, P.A., Colotta, V., Varani, K., 2016. Design, synthesis, and pharmacological characterization of 2-(2-Furanyl)thiazolo[5,4-d]pyrimidine-5,7-diamine derivatives: new highly potent A2A adenosine receptor inverse agonists with antinociceptive activity. J. Med. Chem. 59, 10564–10576. https://doi.org/10.1021/ACS.JMEDCHEM.6B01068.
Vaes, J.E.G., Brandt, M.J.V., Wanders, N., Benders, M.J.N.L., de Theije, Gressens, P., Nijboer, C.H., 2021. The impact of trophic and immunomodulatory factors on oligodendrocyte maturation: Potential treatments for encephalopathy of prematurity. Glia 69, 1311–1340. https://doi.org/10.1002/glia.23939.
Varano, F., Catarzi, D., Vigiani, E., Vincenzi, F., Pasquini, S., Varani, K., Colotta, V., 2020a. Piperazine-and piperidine-containing thiazolo[5,4-d]pyrimidine derivatives as new potent and selective adenosine a2a receptor inverse agonists. Pharmaceuticals 13, 1–19. https://doi.org/10.3390/PH13080161.
Varano, F., Catarzi, D., Vincenzi, F., Pasquini, S., Pelletier, J., Lopes Rangel Fietto, J., Espindola Gelsleichter, N., Sarlandie, M., Guilbaud, A., Sévigny, J., Varani, K., Colotta, V., 2020b. Structural investigation on thiazolo[5,4-d]pyrimidines to obtain dual-acting blockers of CD73 and adenosine A2A receptor as potential antitumor agents. Bioorg Med Chem Lett 30. https://doi.org/10.1016/J.BMCL.2020.127067.
Watanabe, K., Tanaka, M., Yuki, S., Hirai, M., Yamamoto, Y., 2018. How is edaravone effective against acute ischemic stroke and amyotrophic lateral sclerosis? J. Clin. Biochem. Nutr. 62, 20–38. https://doi.org/10.3164/JCBN.17-62.
Xie, W., Uchida, H., Nagai, J., Ueda, M., Chun, J., Ueda, H., 2010. Calpain-mediated down-regulation of myelin-associated glycoprotein in lysophosphatidic acid-induced neuropathic pain. J. Neurochem. 113 (4), 1002–1011. https://doi.org/10.1111/j.1471-4159.2010.06664.x. PMID: 20420580; PMCID: PMC2908211.
Yao, S.-Q., Li, Z.-Z., Huang, Q.-Y., Li, F., Wang, Z.-W., Augusto, E., He, J.-C., Wang, X.-T., Chen, J.-F., Zheng, R.-Y., 2012. Genetic inactivation of the adenosine A $_{2A}$ receptor exacerbates brain damage in mice with experimental autoimmune encephalomyelitis. J. Neurochem. 123, 100–112. https://doi.org/10.1111/j.1471-4159.2012.07807.x.
Zurbriggen, A., Vandevelde, M., Steck, A., Angst, B., 1984. Myelin-associated glycoprotein is produced before myelin basic protein in cultured oligodendrocytes. J. Neuroimmunol. 6 (1), 41–49. https://doi.org/10.1016/0165-5728(84)90041-9. PMID: 6200496.